



Pressure-induced high-temperature superconductivity retained without pressure in FeSe single crystals

Liangzi Deng^{a,b,1}, Trevor Bontke^{a,b}, Rabin Dahal^{a,b}, Yu Xie^{c,d}, Bin Gao^e, Xue Li^{c,d}, Ketao Yin^f, Melissa Gooch^{a,b}, Donald Rolston^{a,b}, Tong Chen^e, Zheng Wu^{a,b}, Yanming Ma^{c,d}, Pengcheng Dai^e, and Ching-Wu Chu^{a,b,g,1}

^aDepartment of Physics, University of Houston, Houston, TX 77204; ^bTexas Center for Superconductivity, University of Houston, Houston, TX 77204; ^cInternational Center for Computational Method and Software, College of Physics, Jilin University, Changchun 130012, China; ^dState Key Laboratory of Superhard Materials, College of Physics, Jilin University, Changchun 130012, China; ^eDepartment of Physics and Astronomy, Rice University, Houston, TX 77005; ^fSchool of Physics and Electronic Engineering, Linyi University, Linyi 276005, China; and ^gLawrence Berkeley National Laboratory, Berkeley, CA 94720

Contributed by Ching-Wu Chu, June 10, 2021 (sent for review May 13, 2021; reviewed by Qiang Li and James S. Schilling)

To raise the superconducting-transition temperature (T_c) has been the driving force for the long-sustained effort in superconductivity research. Recent progress in hydrides with T_c s up to 287 K under pressure of 267 GPa has heralded a new era of room temperature superconductivity (RTS) with immense technological promise. Indeed, RTS will lift the temperature barrier for the ubiquitous application of superconductivity. Unfortunately, formidable pressure is required to attain such high T_c s. The most effective relief to this impasse is to remove the pressure needed while retaining the pressure-induced T_c without pressure. Here, we show such a possibility in the pure and doped high-temperature superconductor (HTS) FeSe by retaining, at ambient pressure via pressure quenching (PQ), its T_c up to 37 K (quadrupling that of a pristine FeSe at ambient) and other pressure-induced phases. We have also observed that some phases remain stable without pressure at up to 300 K and for at least 7 d. The observations are in qualitative agreement with our ab initio simulations using the solid-state nudged elastic band (SSNEB) method. We strongly believe that the PQ technique developed here can be adapted to the RTS hydrides and other materials of value with minimal effort.

FeSe | high-temperature superconductivity | high pressure | pressure quench | retention

The vast impact of room temperature superconductivity (RTS) on humanity is limited only by the imagination. Recent reports show that RTS is indeed within reach, although only under high pressure (HP). For instance, superconducting-transition temperatures (T_c s) above 200 K have been reported in unstable molecular solids (hydrides), i.e., up to 203 K in H_3S under 155 GPa (1, 2), up to 260 K in LaH_{10} under 190 GPa (3–5), up to 287 K in C–H–S under 267 GPa (6), and potentially well above room temperature in La–H under 158 GPa after thermal cycling (7); earlier, T_c up to 164 K was reported in the stable cuprate high-temperature superconductor (HTS) $HgBa_2Ca_2Cu_3O_{8+\delta}$ under 31 GPa (8, 9). While record-high T_c s reported to date fall into practical cryogenic regimes for applications, the HP required to attain these superconducting states renders them impractical for significant applications or for scientific inquiries. The challenge is not restricted to further increasing the superconducting transition temperature under extreme conditions and must now include concentrated efforts to lower, and better yet remove, the applied pressure (P_A) required. Retaining the pressure-enhanced or -induced high- T_c superconducting (SC) phase (1–12) without pressure will effectively meet this challenge.

It has been shown that most of the alloys used in industrial applications are actually metastable at room temperature and atmospheric pressure (13). These metastable phases possess desired and/or enhanced properties that their stable counterparts lack. Examples include diamond and other superhard materials, heavily doped semiconducting materials, certain three-dimensionally printed materials, highly polymeric materials, black phosphorus, etc. They are metastable because they are kinetically stable but thermodynamically not, protected only by an energy barrier (Fig. 1A). By taking advantage

of such energy barriers, lattice and/or electronic, one may therefore be able to stabilize the metastable phase or the “supercooled” state at atmospheric pressure via rapid pressure quenching (PQ) and/or temperature quenching. The energy barrier may be fortified by chemical doping; ionic liquid gating (14); a proper thermodynamic path; and introduction of strains (15), defects (16), or pressure inhomogeneity (17). The pressure-enhanced or -induced SC phase with a high T_c may be considered metastable or supercooled and may be stabilized. Here, we report the successful retention of pressure-enhanced and -induced SC phases at ambient pressure in the Fe-based HTSs via PQ (Fig. 1B) at a chosen quench pressure (P_Q) and quench temperature (T_Q). P_Q is the pressure from which the pressure is rapidly removed to ambient. T_Q is the temperature at which the pressure is removed, and it remains unchanged during the PQ process. We have successfully retained a pressure-enhanced SC phase with a T_c up to 37 K at $P_Q = 4.15$ GPa and $T_Q = 4.2$ K in the SC FeSe and a pressure-induced SC phase with a T_c up to 26.5 K at $P_Q = 6.32$ GPa and $T_Q = 4.2$ K in the non-SC Cu-doped FeSe. We have also retained the insulating phase induced by pressure above ~ 9 GPa in both samples via PQ. The pressure-quenched (PQed) high- T_c phases have also been found to be stable up to ~ 200 K and

Significance

As room temperature superconductivity (RTS) has been reported recently in hydrides at megabar pressures, the grand challenge in superconductivity research and development is no longer restricted to further increasing the superconducting transition temperature under extreme conditions and must now include concentrated efforts to lower, and better yet remove, the applied pressure required. This work addresses directly such a challenge by demonstrating our successful retention of pressure-enhanced and/or -induced superconducting phases and/or semiconducting phases without pressure in single crystals of superconducting FeSe and non-superconducting Cu-doped FeSe. The pressure-quenching technique developed in this work offers the possibility of future practical application and the unraveling of RTS recently detected in hydrides but only under high pressures.

Author contributions: L.D., Z.W., and C.-W.C. designed research; L.D., T.B., R.D., M.G., and D.R. performed research; Y.X., B.G., X.L., K.Y., T.C., Z.W., Y.M., and P.D. contributed new reagents/analytic tools; L.D., T.B., and C.-W.C. analyzed data; L.D. and C.-W.C. wrote the paper; and L.D. and C.-W.C. directed the project.

Reviewers: Q.L., Brookhaven National Laboratory; and J.S.S., Washington University in St. Louis.

The authors declare no competing interest.

Published under the PNAS license.

See online for related content such as Commentaries.

¹To whom correspondence may be addressed. Email: cwchu@uh.edu or ldeng2@central.uh.edu.

This article contains supporting information online at <https://www.pnas.org/lookup/suppl/doi:10.1073/pnas.2108938118/-DCSupplemental>.

Published July 7, 2021.

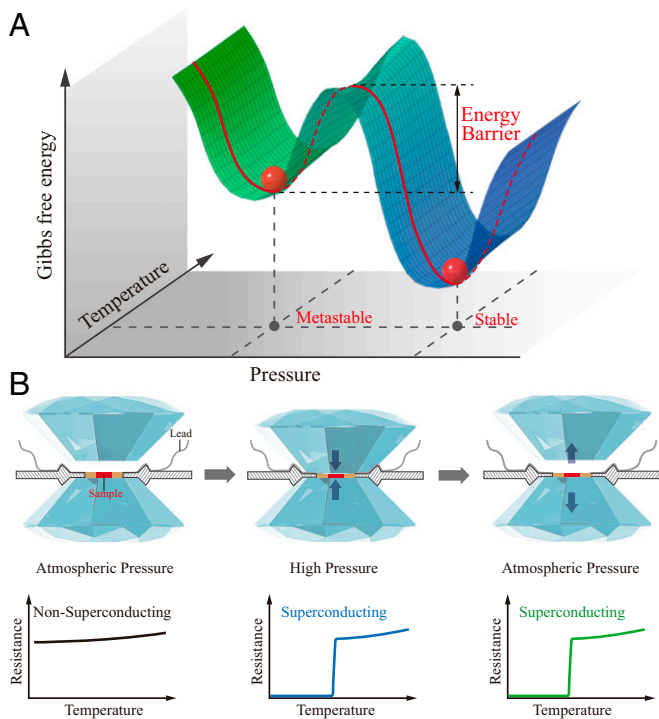


Fig. 1. Schematic diagrams of (A) Gibbs free energy and the energy barrier between the metastable and stable states and (B) the sequence of main experimental steps.

for at least 7 d. Our observations have thus demonstrated that the pressure-enhanced or -induced high- T_c phases in HTSs can be retained at ambient pressure via PQ at a chosen P_Q and T_Q , suggesting a possible realistic path to the ubiquitous applications of the recently reported RTS.

Results and Discussion

In the present study, we have chosen single crystals of the SC FeSe (18) and the non-SC Cu-doped FeSe (19) as model HTSs due to their simple structure and chemistry, as well as their large T_c variation under pressure (20, 21) and their important role in unraveling HTS (22–24). Furthermore, the iron-chalcogenide superconductors have attracted broad interest for applications from high-field magnets to quantum information science. For example, the Majorana zero modes reported in iron-chalcogenide superconductors can potentially be used for building topological qubits (25). The normalized resistance of FeSe and Cu-doped FeSe at 300 K as a function of pressure [$R(P_A)/R(0)$] during pressure increasing and decreasing is displayed in *SI Appendix*, Fig. S1, which shows a clear hysteresis, suggesting that PQ may be possible since thermal hysteresis may provide the energy barrier (Fig. 1A) to retain the HP-induced phases. Preliminary boundaries of the orthorhombic (O)–tetragonal (T)–hexagonal (H) phase transitions of FeSe previously reported (20, 26) are also shown for later discussion. The T–O transition is suppressed from ~ 90 K at ambient pressure to below 4.2 K at ~ 2 GPa, as indicated by the dashed line at *Left* in the same figure. At ambient pressure, $R(T)$ of FeSe shows a sharp SC transition at 9.3 K (SI Appendix, Fig. S2). The transition broadens under pressure, so the $T_c(P)$ cited hereafter refers to the onset temperature as defined in *SI Appendix*, Fig. S2. Fig. 2 (blue squares) displays the T_c -variation of FeSe with P_A : It increases slowly from ~ 9 K at ambient pressure to ~ 15 K below 1.9 GPa; suddenly jumps to ~ 32 K at 1.9 GPa, coinciding with the O–T transition; continues to rise with a broad peak at ~ 40 K around 4 GPa; but finally becomes insulating above ~ 8 GPa as the H phase sets in.

To retain at ambient pressure the above pressure-enhanced T_c of FeSe, we have developed a technique to PQ the sample at different P_{OS} and T_{OS} by rapidly removing the P_A , under which a desired T_c has been first attained, from the sample in the diamond anvil cell, as shown in Fig. 3 A–F. The temperature-dependent resistance of FeSe at different P_A s normalized to those at 70 K, $R(T, P_A)/R(70 \text{ K}, P_A)$, near the superconducting transitions are exemplified in Fig. 3 A and B for $P_{AS} = 4.15$ GPa (close to maximum $T_c \sim 40$ K in the tetragonal phase), and 11.27 GPa (non-SC in the hexagonal phase), respectively. By following different thermal and pressure protocols as specified in the captions, they demonstrate the generation or destruction of the HP SC phase at P_A (blue), the retention at ambient pressure of the PQed (at 4.2 K) HP SC phase (red), and the thermal annealing effect up to 300 K on the PQed (at 4.2 K) HP phase to ascertain its retention (orange), all carried out sequentially.

As is evident from Fig. 3A, the T_c of the FeSe sample has been enhanced from ~ 9 K at ambient pressure to ~ 39 K under 4.15 GPa (blue). After PQ at 4.15 GPa and 4.2 K, a SC transition with a $T_c \sim 37$ K is detected at ambient pressure (red). To show that the 37 K– T_c is indeed attained by PQ, we heated the sample up to 300 K before cooling it back down to 4.2 K and found that the PQed SC transition at 37 K is annealed away and replaced by its pre-PQed one, although at a higher $T_c \sim 20$ K (orange) rather than ~ 9 K, presumably because of an unknown irreversible residual strain effect in the sample (27). Fig. 3B shows that FeSe at 11.27 GPa displays a non-SC transition as expected (blue), as does the PQed sample (red). However, the sample regains its SC transition with a $T_c \sim 20$ K after the PQed phase is annealed off after being heated up to 300 K (orange). To demonstrate the metastability of the PQed SC phases, the SC transition PQed at $P_Q = 4.13$ GPa and $T_Q = 4.2$ K upon sequential thermal cycling to higher temperatures is shown in Fig. 3C. The transition smoothly shifts downward and becomes sharper due to possible reduced fluctuations at lower temperature and/or the possible improved strain condition of the sample upon thermal annealing at higher temperatures. The sudden downward shift in the overall SC transition by ~ 10 K after heating up to ~ 200 K implies that the PQed phase transforms to the pre-PQed FeSe phase (with strain) and is stable up to 200 K. All T_c s of the PQed phases examined at different P_{OS} and $T_Q = 4.2$ K are summarized in Fig. 2 (red circles).

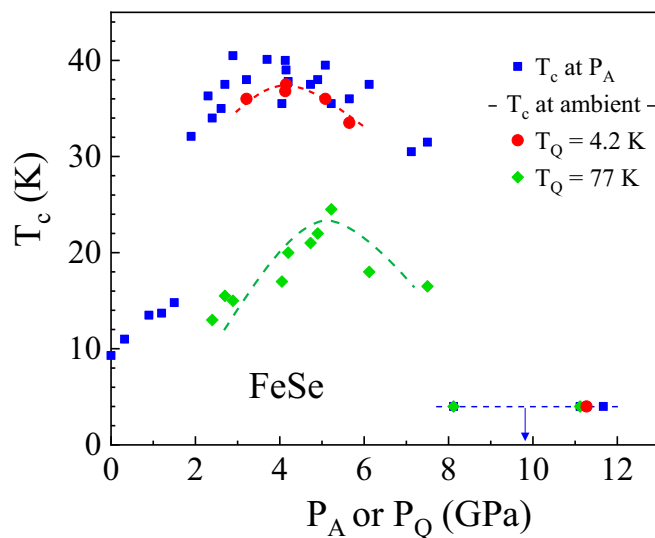


Fig. 2. T_c as a function of P_A or P_Q for single-crystalline FeSe. High-pressure $T_c(P_A)$ at P_A (blue squares), and $T_c(P_Q)$ at ambient pressure for FeSe PQed at P_Q and $T_Q = 4.2$ K (red circles) and $T_Q = 77$ K (green diamonds), respectively.

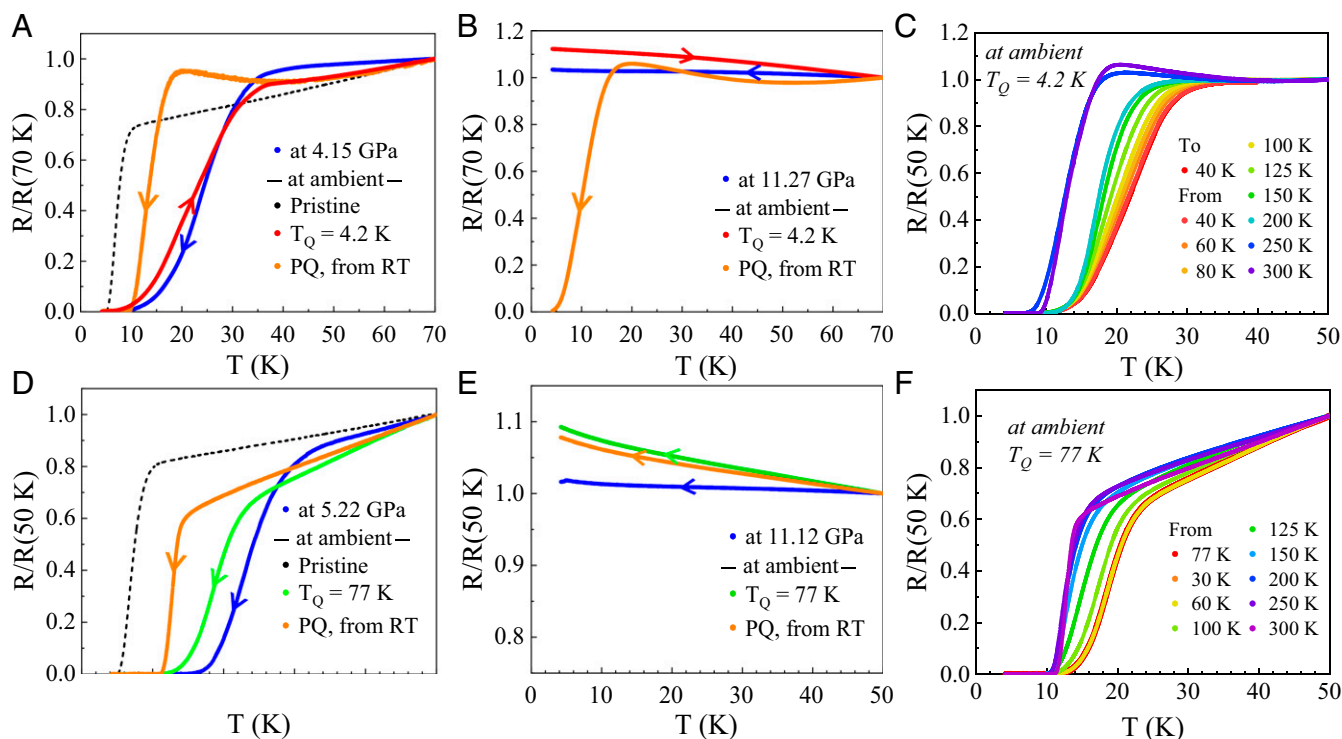


Fig. 3. Pressure quenching (PQ) the single-crystalline FeSe. $R(T)/R(70\text{ K})$ or $R(T)/R(50\text{ K})$ under P_A and at ambient pressure before and after PQ: (A) at $P_A = 4.15$ GPa (blue), and at ambient pressure before PQ on cooling (black), after PQ at 4.15 GPa and 4.2 K on warming (red), and on cooling after warming to 300 K (orange); (B) at $P_A = 11.27$ GPa (blue), and at ambient pressure after PQ at 11.27 GPa and 4.2 K on warming (red) and on cooling after warming to 300 K (orange); (C) after PQ at 4.13 GPa and 4.2 K, warmed to 40 K and sequentially cooled from different temperatures between 40 and 300 K as shown; (D) at $P_A = 5.22$ GPa (blue), and at ambient pressure before PQ on cooling (black), after PQ at 5.22 GPa and 77 K on cooling (green) and on cooling after warming to 300 K (orange); (E) at $P_A = 11.12$ GPa (blue), and at ambient pressure after PQ at 11.12 GPa and 77 K on cooling (green) and on cooling after warming to 300 K (orange); and (F) after PQ at 5.22 GPa and 77 K sequentially cooled from different temperatures between 77 and 300 K as shown.

As mentioned earlier, the PQed phase is metastable, and thus should depend on P_O and T_O and detailed electronic and phonon energy spectra of the materials examined. We have therefore repeated the PQ experiments on FeSe by raising only the T_O to 77 K (Fig. 3 D–F). Fig. 3D shows that the T_c of FeSe before PQ has been enhanced to ~ 37 K at 5.22 GPa (blue); upon PQ, a $T_c \sim 24$ K is retained at ambient pressure (green) in contrast to the 37 K when $T_O = 4.2$ K, as shown in Fig. 3A; and the transition returns to ~ 14 K on cooling after warming to 300 K, showing that the 24 K transition is associated with the PQed phase. Fig. 3E shows that FeSe becomes insulating at 11.12 GPa (blue); the phase is retained at ambient pressure by PQ (green); and the PQed phase remains after heating to 300 K, suggesting that this PQed non-SC phase is stable up to 300 K. The effect of systematic thermal cycling with increasing temperatures on the PQed phase at $P_O = 5.22$ GPa and $T_O = 77$ K is shown in Fig. 3F. All T_c s of the PQ phases examined at different P_O s and $T_O = 77$ K are also summarized in Fig. 2 (green diamonds). They are all lower than those quenched at various P_O and $T_O = 4.2$ K in general agreement with the competition between the instability of the SC state and thermal excitation.

To demonstrate that the retained SC state after PQ in pure FeSe at ambient pressure is not associated with the superconductivity of the pristine FeSe at ambient pressure, we have repeated the PQ experiment on two non-SC Cu-doped FeSe samples ($\text{Fe}_{1.01-x}\text{Cu}_x\text{Se}$ with $x = 0.03$ and 0.035 ; the $x = 0.03$ sample is discussed below unless otherwise noted). As shown in *SI Appendix*, Fig. S2B, Cu-doped FeSe is not SC above 1.2 K below 1.2 GPa (19, 21). Under pressure (Fig. 4, blue squares), it abruptly becomes SC with a $T_c \sim 20$ K at 3.11 GPa (*Inset*, *SI Appendix*, Fig. S2B); T_c continues to increase with increasing P_A and peaks at ~ 27 K under 6.23 GPa; and at 9.65 GPa, only trace superconductivity was detected

down to 1.2 K. Following the same protocols as those for the pure FeSe, we performed PQ on Cu-doped FeSe at different P_O s and T_O s, as exemplified by Fig. 5 A–F. Two examples of $R(T, P_A)/R(50\text{ K}, P_A)$ for Cu-doped FeSe are given in Fig. 5A for $P_{AS} = 6.32$ GPa and 6.16 GPa (close to maximum $T_c \sim 27$ K) PQed at $T_O = 4.2$ K and 77 K, respectively; and in Fig. 5B for 9.65 GPa (non-SC) PQed at $T_O = 77$ K. As is evident from the $R(T, P_A)/R(50\text{ K}, P_A)$ in Fig. 5A, $P_A \sim 6$ GPa has induced a SC state in the non-SC Cu-doped FeSe with a $T_c \sim 26$ K (navy and blue); this SC state has been PQed at $P_O = 6.16$ GPa and $T_O = 4.2$ K (red) and at $P_O = 6.32$ GPa and $T_O = 77$ K (green), respectively. Disappearance of the SC phase after thermal cycling up to 300 K (Fig. 5A, orange and brown) demonstrates that the SC states induced by $P_A \sim 6$ GPa have been retained at ambient pressure with $T_c \sim 26$ K via PQ at 4.2 and 77 K, respectively. As shown in Fig. 5B, $P_A = 9.65$ GPa turns the sample to an insulating state (blue); upon PQ at $T_O = 77$ K, it remains insulating (green); and the sample stays in the non-SC state after thermal cycling to 300 K (orange), suggesting that the insulating state PQed at 9.65 GPa and 77 K is stable up to 300 K. The thermal stability ranges of the PQed SC states at $P_O = 6.08$ GPa and $T_O = 4.2$ K and at $P_O = 5.95$ GPa and $T_O = 77$ K are shown in Fig. 5C and D, respectively. They show that the state PQed at a lower T_O possesses a wider thermal stability range. The anomalies observed in $R(T)$ upon warming right after PQ (Fig. 5E) correlate qualitatively with the thermal stability of the PQed phases (Fig. 5C and D). Fig. 5F demonstrates that the PQed SC phase at $P_O = 6.67$ GPa and $T_O = 77$ K remains unchanged for at least 7 d after thermal cycling between 50 and 4.2 K. All PQed T_c s of Cu-doped FeSe are summarized in Fig. 4. Unlike in their pristine unpressurized state, the two different Cu-doped FeSe samples both behave similarly to FeSe under pressures, but with

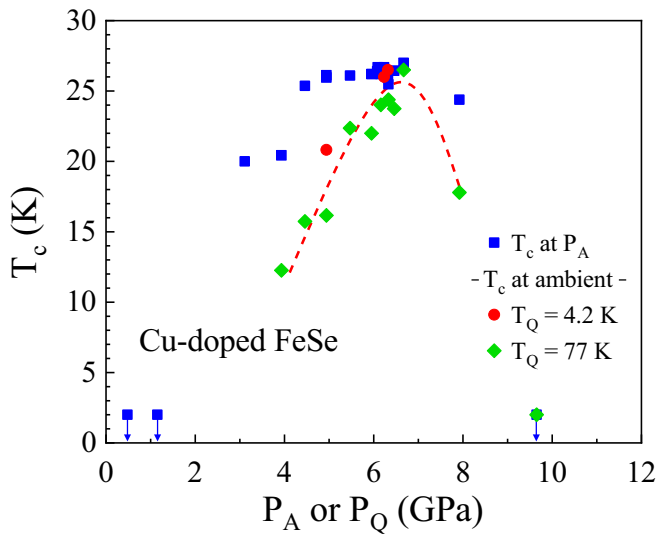


Fig. 4. T_c as a function of P_A or P_Q for single-crystalline Cu-doped FeSe. T_c (P_A) at P_A (blue squares); and at T_c (P_Q) at ambient pressure for the samples PQed at P_Q and $T_Q = 4.2$ K (red circles) and at $T_Q = 77$ K (green diamonds), respectively.

their phase boundaries shifted to higher values, as displayed in Figs. 2 and 4 and *SI Appendix, Fig. S3*, due to the Cu-doping effect. While PQ works for both pure and Cu-doped FeSe in retaining without pressure the pressure-enhanced or -induced SC states, the

effect of T_Q on the T_c of the PQed SC phase for Cu-doped FeSe is smaller than that for FeSe, due to the possible change in the electronic structure resulting from doping. This suggests that doping can help adjust the PQ parameters.

To gain a better understanding of the PQ effects on FeSe, we performed ab initio simulations to evaluate the phase transition energy barriers between different phases via solid-state nudged elastic band (SSNEB) (28). As shown in Fig. 6 *A* and *B*, the phase transition energy barrier between the orthorhombic (29) and tetragonal (30) phases is small. For instance, the energy barrier is 3 meV/atom at 6 GPa, which is lower than the energy barrier of 6 meV/atom at 0 GPa, suggesting that the transition temperature between these two phases at HP should be lower than that at ambient pressure, in agreement with the experimental observations. Nevertheless, the small energy barrier between those two structures ensures that FeSe could preserve the structure phase from one transfer to the other when PQed from above 2 GPa to ambient pressure at low temperatures, as well as the superconductivity. On the other hand, the phase transition energy barrier from the hexagonal (31) to the tetragonal phase is significantly larger, about 0.189 and 0.193 eV/atom at 8 and 11 GPa, respectively (Fig. 6 *C* and *D*). We also noticed that the tetragonal phase is energetically more favorable than the hexagonal phase at simulated pressures. The phase transition between the tetragonal and hexagonal phases will occur at 15 GPa based on our simulation, in agreement with previous calculations (32). The estimated energy barriers are comparable to that between graphite and cubic diamond, around 0.21 eV/atom at 10 GPa (33), suggesting that the hexagonal phase could be preserved during the quenching process once it is formed, as we observed in our experiments. The energy barrier is high enough to prevent

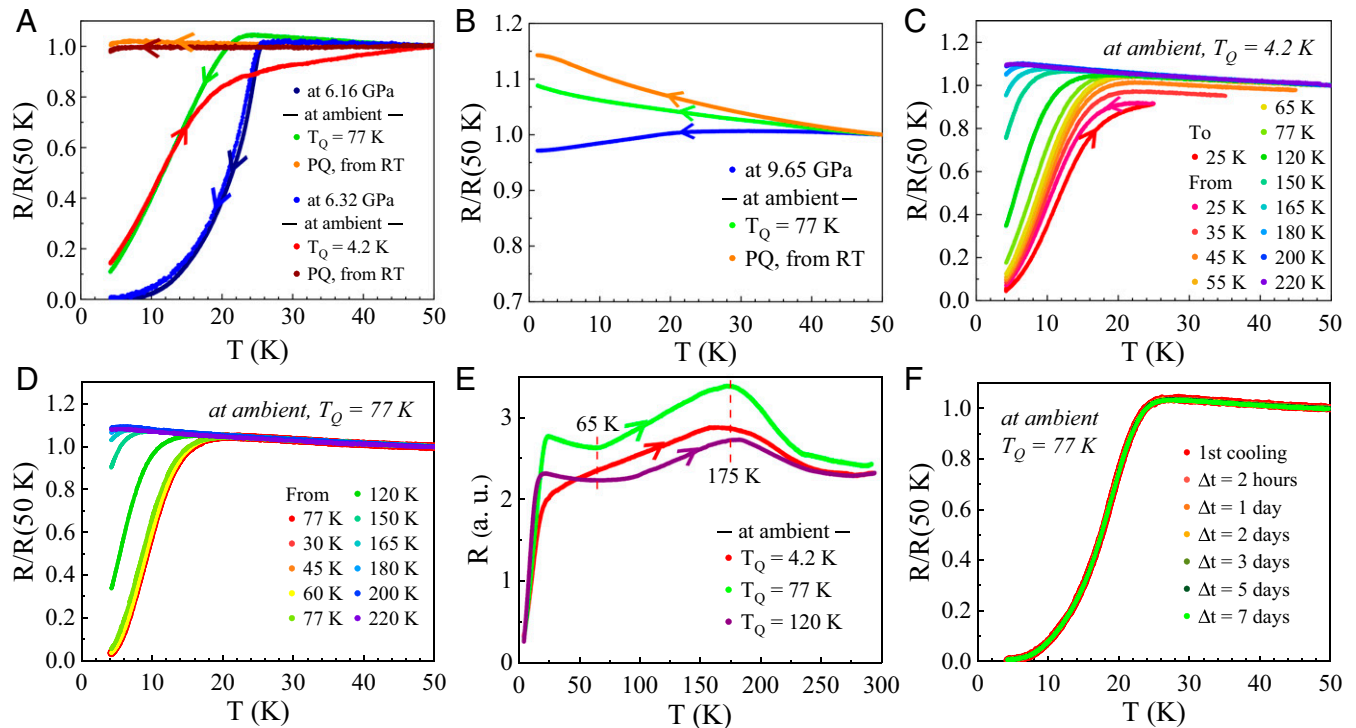


Fig. 5. Pressure quenching (PQ) the single-crystalline Cu-doped FeSe. $R(T)/R(50$ K) under P_A and at ambient pressure after PQ, and testing the stability of the PQed phases: (A) at $P_A = 6.16$ GPa (navy) and 6.32 GPa (blue), and at ambient pressure after PQ at 6.16 GPa and 77 K (green) and at 6.32 GPa and 4.2 K (red), and on cooling after warming to 300 K (orange and brown); (B) at $P_A = 9.65$ GPa (blue), at ambient pressure after PQ at 9.65 GPa and 77 K (green), and on cooling after warming to 300 K (orange); (C) at ambient pressure after PQ at 6.08 GPa and 4.2 K, warmed to 25 K and sequentially cooled from different temperatures between 25 and 220 K as shown; (D) at ambient pressure after PQ at 5.95 GPa and 77 K sequentially cooled from different temperatures between 77 and 220 K as shown; (E) $R(T)$ at ambient pressure for the same sample subjected to different PQ conditions: $P_Q = 6.31$ GPa and $T_Q = 4.2$ K (red), $P_Q = 6.16$ GPa and $T_Q = 77$ K (green), and $P_Q = 6.51$ GPa and $T_Q = 120$ K (purple); and (F) repeated thermal cycling at ambient pressure from 50 K for the sample PQed at 6.67 GPa and 77 K.

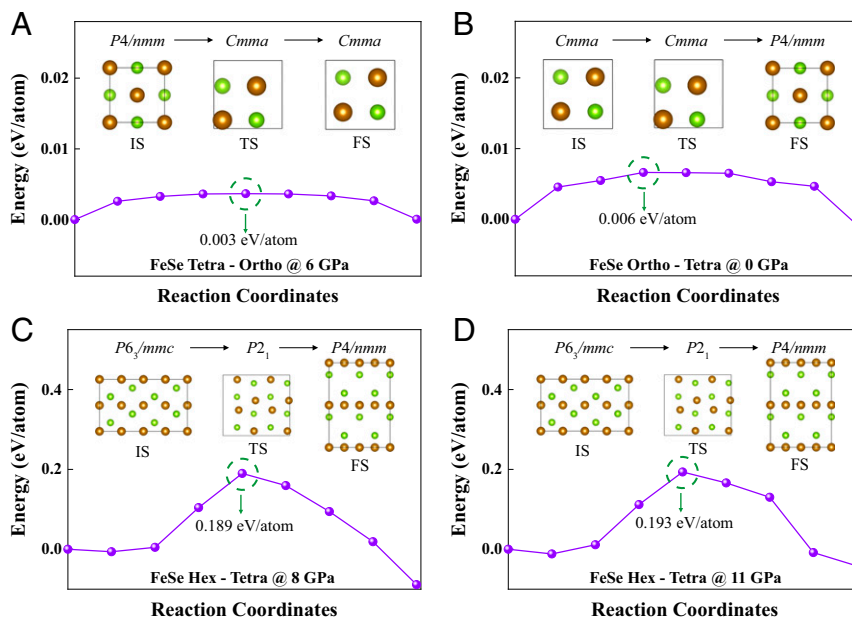


Fig. 6. Energy barrier between different phases of FeSe. Calculated energy barrier from (A) the tetragonal phase to the orthorhombic phase at 6 GPa and (B) the orthorhombic phase to the tetragonal phase at 0 GPa. Calculated energy barrier from the hexagonal phase to the tetragonal phase at (C) 8 GPa and (D) 11 GPa. *Insets* show the side views of corresponding structures including the initial state (IS), the transition state (TS), and the final state (FS) along the *c* axis. The energy barrier was calculated through the SSNEB method in which seven images were used. The arrows show the transition state that is the image with the highest energy and the estimated energy barrier. The green and brown spheres represent elemental Se and Fe, respectively.

FeSe returning to the orthorhombic phase from the hexagonal phase at ambient pressure and 300 K, which is consistent with our experiments at $P_Q = 11.12$ GPa and $T_Q = 77$ K shown in Fig. 3E.

Conclusions

We have demonstrated that the pressure-enhanced or -induced superconducting phases with high T_c and the pressure-induced semiconducting phases in FeSe and Cu-doped FeSe can be stabilized without pressure by PQ at chosen pressures and temperatures. These PQed phases have been shown to be stable at up to 300 K and for up to at least 7 d depending on the quenching conditions. The observations raise the hope that the recently reported RTS in hydrides close to 300 GPa may be retained without pressure, making possible the ubiquitous applications of RTS envisioned.

Materials and Methods

Sample Preparation. Single crystals of $\text{Fe}_{1.01-x}\text{Cu}_x\text{Se}$ ($x = 0, 0.03, \text{ and } 0.035$) were grown using the chemical vapor transport method (34). Stoichiometric Fe (99.9%; Alfa Aesar), Cu (99.9%; Alfa Aesar), and Se (99.5%; Alfa Aesar) powders were thoroughly mixed and loaded into a quartz tube. AlCl_3 (99%; Alfa Aesar) and KCl (99%; Alfa Aesar) powders were added as the transport agents. After the evacuated quartz tube was sealed, it was placed into a two-zone tube furnace, in which the temperatures of the hot and cold positions were maintained at 420 and 330 °C, respectively. After 20 d, single crystals with an average size of $3 \times 3 \times 0.1$ mm³ were grown around the region of the quartz tube's cold zone. Chemical composition was determined by energy-dispersive spectroscopy (EDS) using a Tescan Lyra scanning electron microscope equipped with an EDS detector (Oxford Instruments). The compositions for Cu-doped FeSe single crystals were determined to be $\text{Fe}_{0.98}\text{Cu}_{0.03}\text{Se}$ and $\text{Fe}_{0.975}\text{Cu}_{0.035}\text{Se}$.

Electrical Transport Measurements under Pressure. For resistivity measurements conducted in this investigation, pressure was applied to the samples using a Mao-type symmetric diamond anvil cell (35) with a culet size of 500 μm . The gaskets are made from T301 half-hard stainless-steel sheets with thickness of 300 μm . Each gasket was preindented to $\sim 20\text{--}40$ μm in thickness and was insulated with Stycast 2850FT. The sample's chamber diameter is $\sim 230\text{--}250$ μm , where either sodium chloride or cubic boron nitride is used as the pressure-transmitting medium. Samples were cleaved and cut into thin squares with a

diagonal of ~ 200 μm and thickness of ~ 20 μm . The pressure was determined using the ruby fluorescence scale (36) or the diamond Raman scale (37) at room temperature. The samples' contacts were arranged in a Van der Pauw configuration, and data were collected using a Keithley 6221/2182A Delta Mode System. Measurements were conducted in a homemade cooling system that can be cooled to 1.2 K by pumping on the liquid-helium space. PQ was performed by releasing the screws at target temperatures down to 4.2 K with a small residual pressure $P_R < 0.2$ GPa to maintain the electrical connectivity for resistivity measurements, and the P_R was measured at room temperature.

Theoretical Calculations. Our calculations were performed within the framework of density functional theory via the generalized gradient approximation GGA + U method implemented in the Vienna ab initio simulation package (VASP) (38). The electron-ion interactions were represented by means of the all-electron projector augmented wave method (39), where $3d^64s^2$ and $4s^24p^4$ are treated as the valence electrons for Fe and Se, respectively. We used the Dudarev implementation (40) with on-site coulomb interaction $U = 5.0$ eV and on-site exchange interaction $J = 0.8$ eV (41) to treat the localized 3d electron states. The Perdew-Burke-Ernzerhof functional in the generalized gradient approximation (GGA) was used to describe the exchange-correlation potential (42, 43). The plane-wave energy cutoff of 400 eV and a dense *k*-point grid of spacing $2\pi \times 0.03$ \AA^{-1} in the Monkhorst-Pack scheme were used to sample the Brillouin zone. Structural relaxations were performed with forces converged to less than 0.05 eV/ \AA . To determine the energy barriers, we used the SSNEB (28) implemented in VASP. The NEB path was first constructed by linear interpolation of the atomic coordinates and then relaxed until the forces on all atoms were < 0.05 eV/ \AA . Seven images were simulated between the initial and final states.

Data Availability. All study data are included in the article and/or supporting information.

ACKNOWLEDGMENTS. We thank Prof. L. L. Sun, C. Huang, and J. Guo at the Institute of Physics, Chinese Academy of Sciences, for discussions. The work performed at the Texas Center of Superconductivity at the University of Houston is supported by US Air Force Office of Scientific Research Grants FA9550-15-1-0236 and FA9550-20-1-0068, the T. L. Temple Foundation, the John J. and Rebecca Moores Endowment, and the State of Texas through the Texas Center for Superconductivity at the University of Houston. The FeSe and Cu-doped FeSe single-crystal growth work at Rice University is supported by the US Department of Energy, Basic Energy Sciences, under Contract DE-SC0012311 (P.D.).

1. A. P. Drozdov, M. I. Erements, I. A. Troyan, V. Ksenofontov, S. I. Shylin, Conventional superconductivity at 203 kelvin at high pressures in the sulfur hydride system. *Nature* **525**, 73–76 (2015).
2. I. Troyan *et al.*, Observation of superconductivity in hydrogen sulfide from nuclear resonant scattering. *Science* **351**, 1303–1306 (2016).
3. H. Liu, I. I. Naumov, R. Hoffmann, N. W. Ashcroft, R. J. Hemley, Potential high- T_c superconducting lanthanum and yttrium hydrides at high pressure. *Proc. Natl. Acad. Sci. U.S.A.* **114**, 6990–6995 (2017).
4. M. Somayazulu *et al.*, Evidence for superconductivity above 260 K in lanthanum superhydride at megabar pressures. *Phys. Rev. Lett.* **122**, 027001 (2019).
5. A. P. Drozdov *et al.*, Superconductivity at 250 K in lanthanum hydride under high pressures. *Nature* **569**, 528–531 (2019).
6. E. Snider *et al.*, Room-temperature superconductivity in a carbonaceous sulfur hydride. *Nature* **586**, 373–377 (2020).
7. A. D. Grockowiak *et al.*, Hot hydride superconductivity above 550 K. *arXiv [Preprint]* (2020). <https://arxiv.org/abs/2006.03004> (Accessed 4 June 2020).
8. C. W. Chu *et al.*, Superconductivity above 150 K in $\text{HgBa}_2\text{Ca}_2\text{Cu}_3\text{O}_{8+\delta}$ at high pressures. *Nature* **365**, 323–325 (1993).
9. L. Gao *et al.*, Superconductivity up to 164 K in $\text{HgBa}_2\text{Ca}_m\text{Cu}_m\text{O}_{2m+2+\delta}$ ($m = 1, 2$, and 3) under quasihydrostatic pressures. *Phys. Rev. B Condens. Matter* **50**, 4260–4263 (1994).
10. X. J. Chen *et al.*, Enhancement of superconductivity by pressure-driven competition in electronic order. *Nature* **466**, 950–953 (2010).
11. L. Sun *et al.*, Re-emerging superconductivity at 48 kelvin in iron chalcogenides. *Nature* **483**, 67–69 (2012).
12. L. Deng *et al.*, Higher superconducting transition temperature by breaking the universal pressure relation. *Proc. Natl. Acad. Sci. U.S.A.* **116**, 2004–2008 (2019).
13. P. Duwez, Metastable phases obtained by rapid quenching from the liquid state. *Prog. Solid State Chem.* **3**, 377–400 (1967).
14. C. Zhang *et al.*, Low-temperature charging dynamics of the ionic liquid and its gating effect on $\text{FeSe}_{0.5}\text{Te}_{0.5}$ superconducting films. *ACS Appl. Mater. Interfaces* **11**, 17979–17986 (2019).
15. W. Si *et al.*, High current superconductivity in $\text{FeSe}_{0.5}\text{Te}_{0.5}$ -coated conductors at 30 tesla. *Nat. Commun.* **4**, 1347 (2013).
16. L. Z. Deng *et al.*, Evidence for defect-induced superconductivity up to 49 K in $(\text{Ca}_{1-x}\text{R}_x)\text{Fe}_2\text{As}_2$. *Phys. Rev. B Condens. Matter* **93**, 054513 (2016).
17. F. X. Zhang, W. K. Wang, Crystal structure of germanium quenched from the melt under high pressure. *Phys. Rev. B Condens. Matter* **52**, 3113–3116 (1995).
18. F. C. Hsu *et al.*, Superconductivity in the PbO -type structure $\alpha\text{-FeSe}$. *Proc. Natl. Acad. Sci. U.S.A.* **105**, 14262–14264 (2008).
19. A. J. Williams, T. M. McQueen, V. Ksenofontov, C. Felser, R. J. Cava, The metal-insulator transition in $\text{Fe}_{1.01-x}\text{Cu}_x\text{Se}$. *J. Phys. Condens. Matter* **21**, 305701 (2009).
20. S. Medvedev *et al.*, Electronic and magnetic phase diagram of $\beta\text{-Fe}_{1.01}\text{Se}$ with superconductivity at 36.7 K under pressure. *Nat. Mater.* **8**, 630–633 (2009).
21. L. M. Schoop *et al.*, Pressure-restored superconductivity in Cu-substituted FeSe . *Phys. Rev. B Condens. Matter* **84**, 174505 (2011).
22. Q. Y. Wang *et al.*, Interface-induced high-temperature superconductivity in single unit-cell FeSe films on SrTiO_3 . *Chin. Phys. Lett.* **29**, 037402 (2012).
23. S. He *et al.*, Phase diagram and electronic indication of high-temperature superconductivity at 65 K in single-layer FeSe films. *Nat. Mater.* **12**, 605–610 (2013).
24. L. Z. Deng *et al.*, Meissner and mesoscopic superconducting states in 1–4 unit-cell FeSe films. *Phys. Rev. B Condens. Matter* **90**, 214513 (2014).
25. L. Y. Kong *et al.*, Half-integer level shift of vortex bound states in an iron-based superconductor. *Nat. Phys.* **15**, 1181–1187 (2019).
26. K. Miyoshi *et al.*, Enhanced superconductivity on the tetragonal lattice in FeSe under hydrostatic pressure. *J. Phys. Soc. Jpn.* **83**, 013702 (2014).
27. J. P. Locquet *et al.*, Doubling the critical temperature of $\text{La}_{1.9}\text{Sr}_{0.1}\text{CuO}_4$ using epitaxial strain. *Nature* **394**, 453–456 (1998).
28. D. Sheppard, P. Xiao, W. Chemelewski, D. D. Johnson, G. Henkelman, A generalized solid-state nudged elastic band method. *J. Chem. Phys.* **136**, 074103 (2012).
29. K. Horigane, H. Hiraka, K. Ohoyama, Relationship between structure and superconductivity in $\text{FeSe}_{1-x}\text{Te}_x$. *J. Phys. Soc. Jpn.* **78**, 074718 (2009).
30. G. Haegge, A. L. Kindstroem, Roentgenuntersuchungen am system Eisen-Selen. *Z. Phys. Chem. B Chem. Elemproz. Aufbau Mater.* **22**, 453–464 (1933).
31. T. Kamimura *et al.*, Pressure-induced phase transition in Fe-Se and Fe-S systems with a NiAs -type structure. *J. Magn. Magn. Mater.* **104**, 255–256 (1992).
32. C. Lu, X. Q. Yang, C. Y. Zhu, X. Y. Kuang, Theoretical investigation on the structural and thermodynamic properties of FeSe at high pressure and high temperature. *Dalton Trans.* **41**, 9781–9788 (2012).
33. X. Dong *et al.*, An ab initio study on the transition paths from graphite to diamond under pressure. *J. Phys. Condens. Matter* **25**, 145402 (2013).
34. D. Chareev *et al.*, Single crystal growth and characterization of tetragonal FeSe_{1-x} superconductors. *CrystEngComm* **15**, 1989–1993 (2013).
35. B. Li *et al.*, Diamond anvil cell behavior up to 4 Mbar. *Proc. Natl. Acad. Sci. U.S.A.* **115**, 1713–1717 (2018).
36. H. K. Mao, J. Xu, P. M. Bell, Calibration of the ruby pressure gauge to 800 kbar under quasi-hydrostatic conditions. *J. Geophys. Res.* **91**, 4673–4676 (1986).
37. Y. C. Akahama, H. Kawamura, Pressure calibration of diamond anvil Raman gauge to 310 GPa. *J. Appl. Phys.* **100**, 043516 (2006).
38. G. Kresse, J. Furthmüller, Efficient iterative schemes for ab initio total-energy calculations using a plane-wave basis set. *Phys. Rev. B Condens. Matter* **54**, 11169–11186 (1996).
39. P. E. Blöchl, Projector augmented-wave method. *Phys. Rev. B Condens. Matter* **50**, 17953–17979 (1994).
40. S. L. Dudarev, G. A. Botton, S. Y. Savrasov, C. J. Humphreys, A. P. Sutton, Electron-energy-loss spectra and the structural stability of nickel oxide: An LSDA+U study. *Phys. Rev. B Condens. Matter* **57**, 1505–1509 (1998).
41. J. Zhang *et al.*, Rare helium-bearing compound FeO_2He stabilized at deep-earth conditions. *Phys. Rev. Lett.* **121**, 255703 (2018).
42. J. P. Perdew, Y. Wang, Accurate and simple analytic representation of the electron-gas correlation energy. *Phys. Rev. B Condens. Matter* **45**, 13244–13249 (1992).
43. J. P. Perdew, K. Burke, M. Ernzerhof, Generalized gradient approximation made simple. *Phys. Rev. Lett.* **77**, 3865–3868 (1996).